https://doi.org/10.1595/205651322X16605694237357 *Johnson Matthey Technol. Rev.*, 2022, **66**, (4), 406–417

JOHNSON MATTHEY
TECHNOLOGY REVIEW

technology.matthey.com

Development of New Mixed-Metal Ruthenium and Iridium Oxides as Electrocatalysts for Oxygen Evolution: Part II

Mechanistic understanding and practical considerations

Jasmine A. Clayton, Richard I. Walton*
Department of Chemistry, University of Warwick, Gibbet Hill Road, Coventry, CV4 7AL, UK

***Email:** r.i.walton@warwick.ac.uk

PEER REVIEWED

Received 19th January 2022; Revised 4th May 2022; Accepted 19th May 2022; Online 19th May 2022

We continue our review of recent research into oxides of platinum group metals (pgms), in particular those of ruthenium and iridium, for use as electrocatalysts for the oxygen evolution reaction (OER). In Part I (1), the electrocatalytic splitting of water to oxygen and hydrogen was introduced as a key process in developing future devices for various energy-related applications. A survey of ruthenium and iridium oxide structures for oxygen evolution reaction catalysis was presented. Part II discusses mechanistic details and acid stability of pgm oxides and presents the conclusions and outlook. We highlight emerging work that shows how leaching of the base metals from the multinary compositions occurs during operation to yield active pgm-oxide phases, and how attempts to correlate stability with crystal structure have been made. Implications of these discoveries for the balance of activity and stability needed for effective electrocatalysis in real devices are discussed.

1. Mechanistic Details and Acid Stability of Platinum Group Metal Oxides

There is already a large body of literature on the mechanism of OER electrocatalysis, particularly over binary iridium oxides (2, 3, 4). The process is a complex heterogeneous reaction involving interaction of water with a solid surface under applied potential resulting in evolution of a gas. A number of models have been developed to propose how OER might be broken into fundamental steps to describe the overall phenomenon (5). The purpose of this section is to summarise briefly some of the key, general conclusions of the prior work and then consider the more recent results concerning mechanism that have emerged from the new multinary phases we have introduced in the sections above. As will be appreciated, one important aspect of this work is consideration of the stability of the oxide electrocatalysis, since this is a primary concern when any material is implemented in a real device, where longevity of performance must be a priority (6).

The four electron OER process over a solid surface can be written as a set of one-electron reactions (2, 7, 8). This mechanism has been termed the adsorbates evolution mechanism (AEM), as illustrated in **Figure 1**. The generation of adsorbed hydroperoxide, *OOH, is one of the steps in this process, and this species contains oxygen in oxidation state –1.

For pgm-oxides the involvement of lattice oxide ions in OER has been reported by many groups, with experimental studies of materials

© 2022 Johnson Matthey

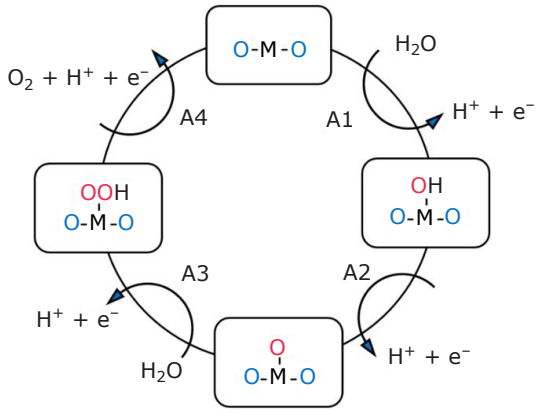

$$* + H_2O \rightarrow *OH + e^- + H^+ \quad (A1)$$

$$*OH \rightarrow *O + e^- + H^+ \quad (A2)$$

$$*O + H_2O \rightarrow *OOH + e^- + H^+ \quad (A3)$$

$$*OOH \rightarrow O_2 + * + e^- + H^+ \quad (A4)$$

Fig. 1. The AEM for OER. * represents a surface-adsorbed species and M is a surface metal site. Adapted with permission from (8). Copyright (2019) American Chemical Society

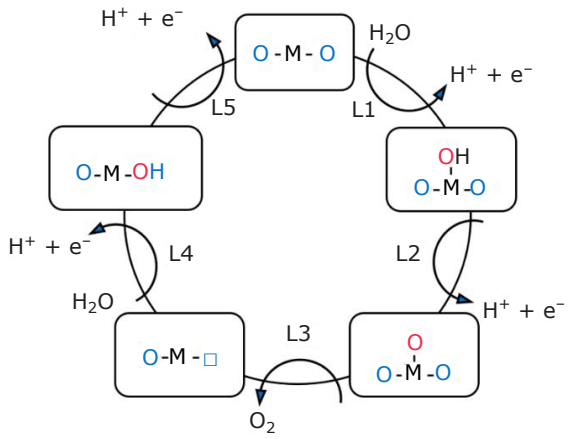

$$* + H_2O \rightarrow *OH + e^- + H^+ \quad (L1)$$

$$*OH \rightarrow *O + e^- + H^+ \quad (L2)$$

$$*O + O_L \rightarrow O_2 + V_o \quad (L3)$$

$$V_o + H_2O \rightarrow *H + e^- + H^+ \quad (L4)$$

$$*H \rightarrow * + e^- + H^+ \quad (L5)$$

Fig. 2. The LOM. * represents a surface-adsorbed species, M is a surface metal site and V_o is a vacant oxide site, shown by □ on the left image. Adapted with permission from (8). Copyright (2019) American Chemical Society

such as IrO_2 and RuO_2 providing evidence for the exchange of water between lattice oxide and water (4, 8). For example, Schweinar *et al.* used isotope labelling and atom probe tomography to show that crystalline IrO_2 surfaces release lattice oxide, resulting in structural change at the surface with dissolution of metal cations and their partial redeposition (9). This mechanism has been termed the lattice-oxygen participation mechanism (LOM) and may be represented as shown in **Figure 2**.

Computational work has revealed that the LOM pathway offers lower kinetic barriers than AEM so provides the possibility of more effective electrocatalysis (10). Other computational work has shown that for perfect crystalline surfaces, the AEM pathway is preferred, but with the introduction of defects the LOM becomes favoured (11). The AEM and LOM may not be distinct situations but may occur simultaneously, to a greater or lesser extent, depending on the surface chemistry of the particular material used as a catalyst. In each case, a change in pgm oxidation state is implied during the OER process, and for IrO_2-based materials this may involve oxidation to Ir^{5+} or Ir^{6+} (12–16), or reduction to Ir^{3+} (17). For less crystalline iridium oxides, there may be a proportion of Ir^{3+} present before electrochemistry is performed (18). In fact these observations are not consistently made in the literature and the role of iridium redox in OER is not universally established: this may be in part because the experimental methods to probe oxidation state change are sensitive to only either the bulk or surface of sample, or have not been implemented *in operando*, but equally it may be the case that not all materials react by the same universal mechanism. It is highly possible that metal oxide surfaces prepared by different routes, with different crystallinity and degree of hydration undergo different changes in response to applied potential in an aqueous acid electrolyte. Although is it clear that surface binding of water must occur during OER, followed by redox chemistry associated with the pgm, another consideration to make is that involvement of electrons from the conduction

 © 2022 Johnson Matthey

band of metallic pgm-oxide may play a role in the catalysis. That is, rather than just the surface pgm cations undergoing oxidation-state change, the whole particle responds by adjustment of the Fermi level of the conduction band. This 'band model' as distinct to the 'bond model' was discussed by Hillman *et al.*, with experimental evidence provided using X-ray absorption spectroscopy of iridium oxide films (19), and some evidence was also found for its role in the OER activity of the pyrochlores $(Na,Ca)_{2-x}Ir_2O_6{\cdot}H_2O$ (13).

As well as the redox chemistry of the pgm, the involvement of oxygen redox in OER has been proven experimentally, with evidence for the formation of electrophilic O^{-1} as a reactive intermediate before the formation of molecular O_2 (20). It has been proposed that the dynamic nature of the iridium framework in amorphous IrO_x imparts the flexibility in iridium oxidation state required for the formation of this active electrophilic oxygen (21). In the case of the LOM, however, the presence of vacant oxide sites leads to weakened binding of the metals, which induces the dissolution of the catalyst (22, 23). Evidence for increased iridium-iridium interactions upon lattice oxide removal has been proposed to account for the relative stability of IrO_2 (24). For RuO_2, the loss of lattice oxygen may occur more readily, leading to greater instability compared to IrO_2 (11), although oxidation to soluble RuO_4 is also an important contributory factor (25).

It is very clear from the work on IrO_2 and RuO_2, in both crystalline and amorphous, hydrated and anhydrous forms, that the surface chemistry is dynamic under acid conditions. The LOM pathway implies stress on the oxide surface that can contribute to amorphisation, dissolution and redeposition of the electrocatalyst (26), i.e. with operating potentials of OER results in reconstruction of the crystal structure. It is highly likely that the active surface layer of the electrocatalyst is amorphous once subjected to electrochemical conditions, and also becomes increasingly hydrous. Relating to this surface restructuring is the loss of surface species into solution, and although some may be redeposited, this dissolution can ultimately lead to loss of the active pgms and eventually failure of the electrocatalysts. Another resulting issue is the interference of any dissolved metal cations with other components of the device: for example interaction with the fluorocarbon polymer electrolyte may inhibit its proton conductivity (27). It is observed that the most active materials for OER electrocatalysis are also the least stable with respect to dissolution (28), and resolving this 'activity–stability conundrum' is an important goal in developing resilient materials with properties optimal for applications (29).

2. Measurement of Oxygen Evolution Performance of Platinum Group Metal Oxides

Before we examine the new OER electrocatalyst materials discovered in the last few years, it is important to consider how performance is measured and assessed. One initial observation is that different conditions may have been applied in the measurement of OER performance: as well as the pH of the electrolyte (usually aqueous $HClO_4$ or H_2SO_4) and the temperature of measurement, the composition of the catalyst layer may not be consistent. In some studies a powdered sample is mixed with carbon as a conducting binder or support, while in other cases an oxide is deposited as a layer or film directly onto a substrate. The surface area and particle size of the catalyst must be considered, and the applied electrochemical conditions (range of potential, sweep rate, number of cycles) must be taken into account, when comparing data from what notionally is the same catalyst. For example, the rate of dissolution of RuO_2 in acid electrolytes depends on its synthesis method, and can vary over several orders of magnitude (30). Notwithstanding these experimental issues, the metrics used to assess performance are not necessarily the same between different reported studies: assignment of a consistent 'figure of merit' is not apparent in the literature on OER electrocatalysts. Parameters used in the literature to assess performance of OER electrocatalysts, include the following (31): (a) the onset potential, the applied potential at which OER is detected; (b) the Tafel slope, which is rate of change of current density, giving information about kinetics of OER; (c) the overpotential, the potential to achieve a specified geometric current density, typically 10 mA cm^{-2}, but which may not reflect intrinsic activity as it does not consider loading or surface area; (d) the mass activity, determined by normalising the catalytic current by the catalyst loading, and may be expressed as mass of catalyst or mass of pgm, to reflect the cost efficiency; (e) Faradaic efficiency, obtained by relating the amount of evolved oxygen to the theoretical amount.

The 'activity' of a catalyst is often the most sought-after property, and it can be seen that this may be quoted in a number of ways, each of which may be dependent on the experimental variables

 © 2022 Johnson Matthey

mentioned above (electrolyte pH, mass loading of catalyst, surface area or choice of support). In terms of stability, a chronopotentiometric hold at constant current density for a chosen period of time, or repeated cyclic voltammetry with specific scan rates for thousands of cycles may provide appropriate measures (31). But, as already discussed, the dissolution of catalyst is a crucial factor. Gieger *et al.* proposed a 'stability number' as a benchmark for assessing stability. Their S–number is defined as the ratio between the amount of evolved oxygen and the amount of dissolved pgm (extracted from ICP-MS data) and this describes how many oxygen molecules are formed per pgm atom lost into the electrolyte (22).

3. Oxygen Evolution Activity of Complex Iridium and Ruthenium Oxides

OER performance data presented for some of the complex ruthenium and iridium oxides have recently been tabulated and compared in some review articles (32, 33, 34). **Table I** summarises some of the activity and stability values reported for a variety of the recently discovered ruthenate and iridate materials. For comparison, similar values for crystalline RuO_2 and IrO_2 are recorded, but it should be noted that while these data are representative, even for these simple binary solids there exists a range of metrics reported in the literature (35). In the case of IrO_2, as noted earlier, amorphous forms of the oxide can be considerably more active than crystalline forms. Despite these difficulties in making quantitative comparisons, it can be observed that many of the recently discovered mixed-metal oxides offer enhanced properties over the binary oxides, with low overpotential required to generate significant current densities, higher specific activities, smaller Tafel slope values, and with more favourable stability. The materials $Cr_{0.6}Ru_{0.4}O_2$, 6H-$SrIrO_3$ and $CaCu_3Ru_4O_{12}$ stand out in this respect. The stability number of Gieger *et al.* has not yet been applied by many authors, but in the case of the proton-exchanged form of the Ruddlesden-Popper phase $H_{3.6}IrO_4{\cdot}3.7H_2O$ (not included in **Table I**) the S-value of $\sim10^5$ was higher than for 6H-$SrIrO_3$ ($\sim10^4$) and $Sr_2Ir_{0.5}Fe_{0.5}O_4$ ($\sim10^3$) when studied under the same conditions, and similar to crystalline (10^6) and amorphous forms of IrO_2 (10^6) (48).

A note of caution should also be made around reported data from 'wet cell' electrochemical measurements, such as in classical rotating disc electrode (RDE) experiments, in that they do not necessarily replicate the activity measured under the real conditions in a device. Frydendal *et al.* pointed out that stability cannot be assessed by electrochemical measurements alone and that complementary methods must be used, in their case monitoring the mass of the electrocatalyst and the release of cations into solution (49). Alia *et al.* found that in tests on iridium oxides that RDEs kinetically underperformed MEAs by at least an order of magnitude and that durability of the catalyst in an MEA could not be estimated from the RDE performance (50). In our own work we observed similar conclusions from a study of substituted RuO_2 materials (51). Others have found that inaccuracies in RDE testing may be due to accumulation of gas bubbles, that lead to inconclusive results regarding stability of electrocatalysts (52, 53). Some authors have proposed standard protocols to allow benchmarking and also to assess suitability for use in real devices (54–56), but for the new materials we have focused on in this review, these rigorous testing protocols are yet to be applied.

Some general observations about the mechanistic information that has emerged in the literature on oxide OER catalysts are also appropriate to make. Early work by Trasatti correlated the overpotential for OER with the enthalpy associated with the transition from MO_x to MO_{x+1} (the 'lower to higher oxide transition') for a set of transition metal oxides and found a volcano plot with RuO_2 and IrO_2 close to the apex (i.e. with lowest overpotential for OER) (57). It was proposed that OER most readily takes place with low coverage of adsorbed intermediates, and so for oxides that are easily oxidised, there is high coverage of adsorbed intermediate and thus high overpotential. It can be concluded from this, and others' work, that the metal-oxygen bond strength is an important factor in determining OER activity.

Although similar considerations have not yet been systematically made for the recently discovered novel complex iridium and ruthenium oxides, in multinary metal oxides the presence of partner metals, as well as the distinctive crystal structures, provides a means of regulating electronic structure. For example, in the pyrochlores $Ln_2Ir_2O_7$ (Ln = praseodymium, neodymium, gadolinium, terbium, holmium), Shang *et al.* found that an increased ionic radius of the lanthanide resulted in enhanced covelancy of the Ir–O bonds *via* broadening of the iridium 5*d* band and increased interaction with the O2*p* band, leading to improved OER activity; this

 © 2022 Johnson Matthey

https://doi.org/10.1595/205651322X16605694237357

Table I Activity and Stability Metrics Reported for Representative Mixed-Iridate and Ruthenates with Crystalline RuO_2 and IrO_2 for Comparison

Electrocatalyst	Structure type	Substrate[a]	Electrolyte	Overpotential η (10 mA cm^{-2}), mV	Specific activity	Tafel slope, mV dec^{-1}	Stability	Reference
RuO_2	Rutile	GCE	0.5 M H_2SO_4	316	11.4 A g_{Ru}^{-1} 0.23 mA cm^{-2}_{oxide} @1.5 V	67	1 h at 10 mA cm^{-2}	(35)
IrO_2	Rutile	GCE	0.1 M $HClO_4$	300	< 0.05 11.4 A g_{Ir}^{-1} @1.5 V	78	< 8 h at 10 mA cm^{-2}	(36)
$Ir_{0.7}Ru_{0.3}O_2$	Rutile	GCE	0.5 M H_2SO_4	336 mV (5 mA cm^{-2})	~6 Ag^{-1} @1.8 V	60.4	> 400 h 1 A cm^{-2} at 80°C in a MEA	(37)
$Cr_{0.6}Ru_{0.4}O_2$	Rutile	GCE	0.5 M H_2SO_4	178	~0.17 cm^{-2}_{oxide} @1.45 V	58	> 10 h at 10 mA cm^{-2}	(38)
6H-$SrIrO_3$	Hexagonal perovskite	GCE	0.5 M H_2SO_4	248	76 A g_{Ir}^{-1} @ 1.525 V	not quoted	> 30 h at 10 mA cm^{-2} ~1.3% of total Sr leached and 0% of Ir leached	(39)
$Ba_3TiIr_2O_9$	Hexagonal perovskite	GCE	0.1 M $HClO_4$	275	250 A g_{Ir}^{-1} @1.53 V	45.7	> 20 h at 10 mA cm^{-2} 2.1% Ba 1.6% Ti, 0% Ir leached after 1 h	(40)
IrO_x-$SrIrO_3$	Perovskite	–	0.5 M H_2SO_4	270	10 mA cm^{-2}_{oxide} @1.5 V	~38	> 30 h at 10 mA cm^{-2}	(41)
$Ba_2PrIr_2O_6$	Perovskite	Au	0.1 M $HClO_4$	270	1 mA cm^{-2}	~54 between 1.5 V and 1.6 V; 106 > 1.6 V	~ 1 h at 10 mA cm^{-2}, leaching at 1.55 V: 14.2% Ba; 0.8% Ir; 11.3% Pr	(42)
La_2LiIrO_6	Perovskite	GCE	0.1 M H_2SO_4	~350	0.7 mA cm^{-2}_{oxide} @1.5 V	50	Surface reconstruction occurs	(43)
$CaCu_3Ru_4O_{12}$	Perovskite	GCE	0.5 M H_2SO_4	171	1942 A g_{Ru}^{-1} 22.1 mA cm^{-2}_{oxide} @1.5 V	40	> 24 h at 10 mA cm^{-2}	(35)
$Bi_2Ir_2O_7$	Pyrochlore	Au	1 M H_2SO_4	~355	~1.9 A g_{Ir}^{-1}	45	1000 electrochemical cycles	(44)
$Pr_2Ir_2O_7$	Pyrochlore	GCE	0.1 M $HClO_4$	300	13.3 mA cm^{-2}_{oxide} 424.5 A g_{Ir}^{-1}	~50	1000 cycles at 10 mA cm^{-2} disk	(45)
Porous $Y_2[Ru_{1.6}Y_{0.4}]O_{7-\delta}$	Pyrochlore	GCE	0.1 M $HClO_4$	270 (18.1 mA cm^{-2})	~2.2 mA cm^{-2}_{oxide} @1.5 V	37	Not reported	(46)
$K_{0.25}IrO_2$	Hollandite	Ti	0.1 M $HClO_4$	350	~12.2 A g_{Ir}^{-1} @1.53 V	65	> 4 h @ 1.43 V	(47)

[a]GCE = glassy carbon electrode

© 2022 Johnson Matthey

was accompanied by increased conductivity owing to an insulator to metal transition (45). Hubert *et al.* found that among the $A_2Ru_2O_7$ a longer Ru–O bond and a weaker interaction of the Ru 4*d* and O2*p* orbitals compared with RuO_2 resulted in enhanced initial activity (58). On the other hand Abbot *et al.* noted that the OER activity of each pyrochlore series (i.e., iridate or ruthenate) generally improves as the size of the A-site cation decreases (59). These conflicting observations suggest that structure property relationships are more complex than merely a consideration of bulk crystal structure, and understanding of surface chemistry, and how this arises from preparative method also needs a greater consideration.

Considering the LOM mechanism for OER, where lattice oxide is removed to create a vacant site, the presence of oxide defects can also be considered a principle for the design of effective electrocatalysts. Thus preparation of materials that purposefully contain oxide defects is a strategy for optimisation of activity: this was demonstrated in the case of the pyrochore $Y_2[Ru_{1.6}Y_{0.4}]O_{7-\delta}$, where replacement of some B-site Ru^{4+} by Y^{3+} results in oxide-ion deficiency, albeit accompanied by enhanced covalency of the Ru–O bonds owing to some oxidation of Ru^{4+} to Ru^{5+}, giving higher activity than the parent $Y_2Ru_2O_7$ (46). Likewise, replacing Y^{3+} by Ba^{2+} in $Y_2Ru_2O_7$ generates oxygen vacancies as well as oxidation of ruthenium, thus boosting the OER performance (60). A similar effect was seen in $Y_{1.7}Sr_{0.3}Ru_2O_7$ with the additional effect of increased Ru–O covalency decreasing the charge transfer energy to accelerate interfacial charge transfer kinetics (61). For the materials $Y_{1.8}M_{0.2}Ru_2O_{7-\delta}$ (M = copper, cobalt, nickel, iron, yttrium) the substituent cations were used to purposely tailor the concentration of oxide vacancies and to enhance OER activity (62). Recently, fluorination of the pyrochlore $Y_2Ru_2O_{7-\delta}$ has been proposed as a means of increasing the concentration of oxide-ion defects (63). For the double perovskite La_2LiIrO_6 a unique mechanism for OER activity has been proposed in which the material is activated in acid conditions, by initial extraction of Li^+, to yield Ir^{6+}, leading to migration of cations to the surface and activation of surface oxide, with further steps involving lattice oxide participation, **Figure 3** (43).

Dissolution of the new iridate and ruthenate oxides has been an important part of their study, and just as with the earlier work on IrO_2 and RuO_2, it is becoming apparent that significant surface reconstruction plays an important role in their activity as OER electrocatalysts. For IrO_2 there is

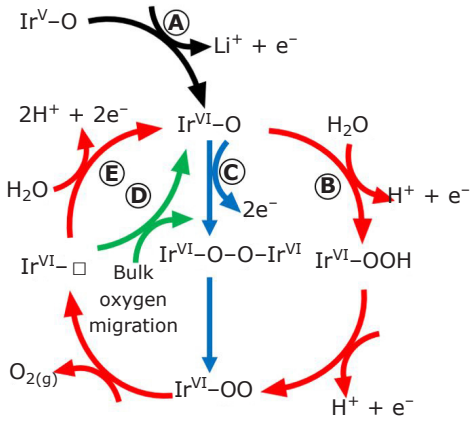

Fig. 3. Mechanism of OER electrocatalysis proposed for La_2LiIrO_6. The first step, **A**, is an activation of the surface in which Li^+ is removed from the structure with oxidation of Ir^V to Ir^{VI}. This is followed by formation of an O–O bond by either reaction with water in step **B** or pairing of surface oxygens in step **C**, leading to oxygen release that creates vacancies (□) that are filled by either migration of crystal oxides in step **D** or reaction with water at the surface in step **E**. Adapted with permission from Springer Nature Customer Service Centre: Springer Nature (43), Copyright (2016)

now a body of work on degradation mechanism under acid conditions, including both experimental and computational studies (23, 64–66). During the degradation of IrO_2, it is concluded that redox chemistry of iridium takes place, and this is intimately connected with the chemistry of the electrocatalysis process (64). Kasian proposed the possible pathways of iridium dissolution, **Figure 4**, where release of soluble iridium species, such as $[IrO_4]^{2-}$ and Ir^{3+} conceivably occurs at different points on the OER cycle (16). While it is likely that similar degradation pathways may occur during the use of the new mixed-metal oxide electrocatalysts that have recently been discovered, at present there are no experimental data available to propose mechanism to the same level of detail. It may also be the case that there is not a common mechanism at play for all materials, given the variety of crystal chemistries.

In the case of pyrochlores, Hubert *et al.* observed that the OER activity of $A_2Ru_2O_7$ catalysts changed over time and is accompanied by both A-site and ruthenium dissolution at different relative rates depending on the identity of the A-site (58). In our own work on $(Na,Ca)_{2-x}Ir_2O_6{\cdot}nH_2O$ pyrochlores, we found that upon immersion in concentrated H_2SO_4 almost complete removal of the A-site sodium and calcium takes place to leave a poorly crystalline material that still resembles the pyrochlore

 © 2022 Johnson Matthey

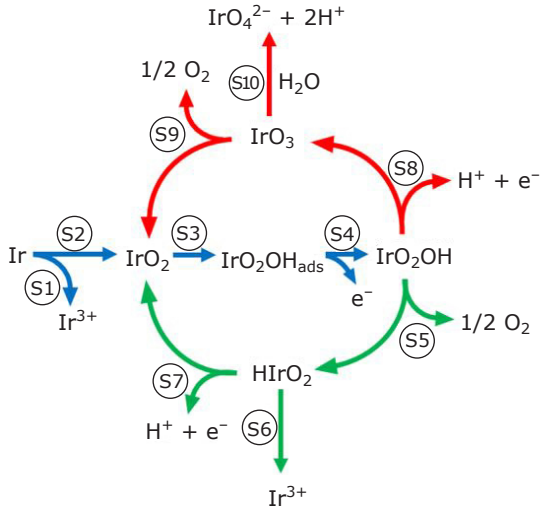

(S1) $Ir \rightleftharpoons Ir^{3+} + 3e^-$

(S2) $Ir + 2H_2O \rightleftharpoons IrO_2 + 4H^+ + 4e^-$

(S3) $IrO_2 + H_2O \rightleftharpoons IrO_2OH_{ads} + H^+$

(S4) $IrO_2OH_{ads} \rightleftharpoons IrO_2OH + e^-$

(S5) $2IrO_2OH \rightleftharpoons 2HIrO_2 + O_2$

(S6) $HIrO_2 + 3H^+ \rightleftharpoons Ir^{3+} + 2H_2O$

(S7) $HIrO_2 \rightleftharpoons IrO_2 + H^+ + e^-$

(S8) $IrO_2OH \rightleftharpoons IrO_3 + H^+ + e^-$

(S9) $2IrO_3 \rightleftharpoons 2IrO_2 + O_2$

(S10) $IrO_3 + H_2O \rightleftharpoons IrO_4^{2-} + 2H^+$

Fig. 4. Possible mechanism for the dissolution of iridium from IrO_2 during OER electrocatalysts in aqueous acid solution, which may result in the formation of solution Ir^{3+} or $[IrO_4]^{2-}$. Figure adapted from (16) under a Creative Commons Attribution-NonCommercial 4.0 International License (CC BY-NC 4.0)

structure and with charge balance provided by protons that are accommodated as bridging OH groups in the pyrochlore lattice (67). Thus proton exchange provides a mechanism to counter the leaching of cations and may indeed allow the effective operation of the electrocatalyst, although this idea needs further investigation. Exchange of cations for protons, prior to use in electrocatalysis, has been applied to form active materials, in the case of $H_{3.6}IrO_4 \cdot 3.7H_2O$ prepared from Ruddlesden-Popper $SrIr_2O_4$ (48).

For the perovskite $SrIrO_3$, grown as thin films as a pseudo cubic phase, Seitz *et al.* showed that the active electrocatalyst after exposure to electrochemical potential in acid was actually IrO_x/$SrIrO_3$ formed from strontium leaching from the surface layers of $SrIrO_3$, and this outperformed binary oxides of iridium or ruthenium (41). Leaching of praseodymium and barium from the double perovskite Ba_2PrIrO_6 was accompanied by only negligible leaching of iridium, and gave a surface enriched in Ir^{5+} (42), while leaching of Y^{3+} from the pyrochlore $Y_2Ir_2O_7$ gave an active iridium-oxide layer (68). In other complex iridium oxides the importance of the leaching of partner ions is being recognised in the formation of the most active catalysts (69–74). These collective results, from iridates with a variety of crystal structures, illustrate how the partner metal cations in multinary oxides can be preferentially lost into the acid electrolyte to leave behind a stabilised iridium oxide surface, or amorphous particles of IrO_x anchored on a support. Surface restructuring is a key part of the nature of the iridate electrocatalysts, and recent studies have begun to investigate the atomic-scale mechanism of these processes (75). It is likely that ruthenates behave similarly, and electrochemical leaching of strontium from $SrRuO_3$ produced RuO_2 clusters with favourable OER activity (76).

While leaching of metal cations from mixed-metal oxides may simply be expected to leave active IrO_x and RuO_x particles, as could be prepared by other routes, it can be seen that in fact the multinary oxides offer distinctive properties. For example, as noted above for La_2LiIrO_6, delithiation increases iridium oxidation state to activate the surface for OER, while for Ruddlesden-Popper and pyrochlore materials the ability to accommodate protons yields robust materials with acid stability.

In terms of relating crystal structure to OER performance, Song *et al.* studied 11 different iridates, representative of the materials we surveyed in Part I (1), including pyrochlores, perovskites and Ruddlesden-Popper phases, and compared their OER activity to IrO_2 (77). Despite having different crystal chemistry, all materials show similar OER activity, however their stability upon repeated cycling showed a remarkable relationship to crystal structure. Those with crystal structures with predominance of face- and edge-sharing connectivity of IrO_6 octahedra offered highest stability, such as hexagonal perovskites, whereas the materials consisting of corner-shared or isolated octahedra, such as Sr_4IrO_6, gave rapid structural collapse and poor electrochemical cyclability. Even the most stable phases showed

 © 2022 Johnson Matthey

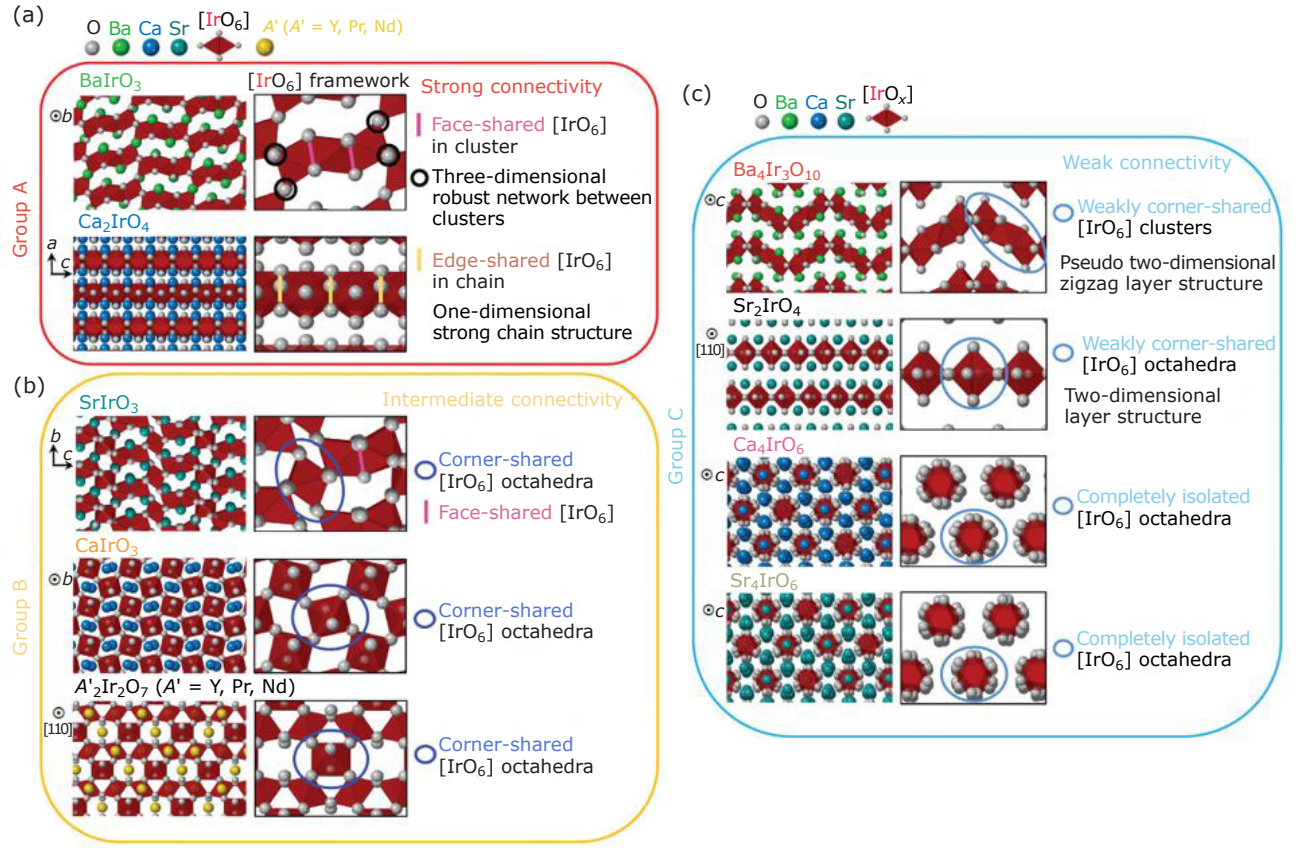

Fig. 5. Three classes of materials to categorise iridates proposed by Song *et al.*: (a) Group A are the most robust materials under acidic OER conditions, giving rise to iridium-rich amorphous layers; (b) Group B are less robust and yield thin iridium-rich layers; (c) Group C are subject to rapid leaching of cations resulting in dissolution. Republished with permission of The Royal Society of Chemistry, from (77); permission conveyed through Copyright Clearance Center, Inc

leaching of the base metal cations and formation of an iridium-rich surface. Song *et al.* classified the structures into three types, **Figure 5**, to relate their stability to crystal structure.

Separately, Yang *et al.* have noted that structures consisting of face-shared IrO_6 octahedra exhibit superior catalytic activity to those that contain corner-shared IrO_6 octahedra due to the weakened surface Ir–O bonding, which lowers the energy barrier of the potential-determining step (39). It has also been observed that highly distorted IrO_6 octahedra tend to be more active than regular IrO_6 octahedra (36), and similar observations about local structural distortion have been made by others, as noted above (78, 79). Taken together, these conclusions suggest some design principles for targeted preparation of materials that are stable in acid solution.

Finally, it is important to consider that as well as the inherent activity and stability of the oxide electrocatalyst, the nature of the catalyst support is important to consider, since this may modify the activity, ideally to provide further stability without loss in activity. This has been recently explored in the case of IrO_2: for example, in the case of titanium metal supports, if the temperature of calcination was too high then migration of titanium into the iridium oxide resulted in loss in electrocatalytic performance (80), the support may allow the oxidation state of iridium to be adjusted in the case of amorphous IrO_x (81), and the choice of support can provide stability to IrO_x nanoparticles (82). Similar considerations are likely to apply to the new mixed-metal oxides produced, but this is yet to be studied.

4. Conclusions and Outlook

In the past few years, a large set of complex oxides of ruthenium and of iridium have been prepared for study as electrocatalysts in acid electrolytes for the OER. Many of these materials have activities that apparently match or surpass that of IrO_2, although as we have highlighted comparison of

 © 2022 Johnson Matthey

reported activity data between literature studies is not always straightforward. The issue of long-term stability needs also to be considered, and several recent works have highlighted the need for proper benchmarking of OER catalysts. We also note that many of the emerging materials have not yet been tested in real devices, and initial findings are based on simple solution electrochemical measurements. There is clearly much work to be done to prove the value of the new materials in realistic conditions, where stability in the presence of other device components requires careful investigation towards scale-up to produce working devices (83). The synthetic route to materials is also important to emphasise, not only in targeting new materials in a rational way, but also when considering that materials must be prepared by a method applicable for manufacture at a suitable scale in a form for processing into devices. Our review highlights some of the diverse synthetic chemistry methods already employed, which suggests that there is opportunity still for discovery of new phases, and that some of the solution-mediated synthesis may allow control of crystal morphology and be suited for scale-up.

Mechanistic understanding is challenging for heterogeneous catalysis in general, but particularly for an electrocatalyst under conditions of device operation, and computation may play a role here, as highlighted for the case of binary IrO_2 and RuO_2 materials. Some interesting structure-property relationships are emerging now that a set of materials is available for consideration, particulary among the iridates that have been studied. Here, a relationship between local atomic connectivity and catalytic behaviour is becoming apparent, with suggestions that certain structural motifs allow the desired balance between activity and durability to be reached. Leaching of the partner metal cation in multinary phases is a common emerging theme, and while this may lead to active iridium-rich surfaces, the fate of the released cations in a real electrochemical device is yet to be established. The role of protons in this leaching is an aspect that warrants further investigation, since this might provide a dynamic mechanism of charge balance. Another structural aspect that has emerged is the role of oxide-ion vacancies and how creation of high-levels of these defects by elemental substitution can lead to enhanced electrocatalytic activity: there are possibilities in extending this work to explore a much wider susbtitutional chemistry, for example by anion replacement to give oxide-substituted materials, as shown recently for sulfur incorporation in $SrIrO_3$ (84).

Another area of research direction for consideration is the exploitation of interfacial effects, where judicious choice of partner materials may lead to a cooperative enhancement of electrocatalysis (8). For example, it has been recently been shown that a Ru/IrO_2 composite could be tuned by addition of small amounts of manganese to moderate the oxidation states of the pgm, and obtain high OER activity in an MEA device, assigned to interfacial enhancement (85). A related opportunity lies in using conducting oxides of iridium and ruthenium, such as pyrochlores, as supports for metallic nanoparticles (86). The role of the substrate and catalyst-support interactions is likely to be of importance in optimising the activity stability-balance in future work.

Finally, we emphasise that quantitative benchmarking of electrocatalyst performance must be considered in future work. A number of different metrics have so far been used to report activity and stability, notwithstanding that catalysts may not have been tested under comparative conditions. Future work must also consider the mechanism of degradation of the materials in order to optimise properties. At present, although it is clear that materials with highly desirable properties for OER electrocatalysis have been discovered in the past few years, the most appropriate materials for practical application have not yet been unambiguously identified.

Acknowledgements

We thank our colleagues at Johnson Matthey, particularly the group of Jonathan Sharman, for their continued collaboration in work in this field. Jasmine Clayton thanks Johnson Matthey for part funding of a PhD studentship with the EPSRC Doctoral Training Partnership award EP/R513374/1. Richard Walton thanks the Royal Society for provision of an Industry Fellowship with Johnson Matthey during which some of ideas in this article were developed.

References

1. J. A. Clayton and R. I. Walton, *Johnson Matthey Technol. Rev.*, 2022, **66**, (4), 393
2. Z. Pu, T. Liu, G. Zhang, H. Ranganathan, Z. Chen and S. Sun, *ChemSusChem*, 2021, **14**, (21), 4636
3. T. Reier, H. N. Nong, D. Teschner, R. Schlögl and P. Strasser, *Adv. Energy Mater.*, 2016, **7**, (1), 1601275

 © 2022 Johnson Matthey

4. T. Naito, T. Shinagawa, T. Nishimoto and K. Takanabe, *Inorg. Chem. Front.*, 2021, **8**, (11), 2900
5. L. J. Falling, J. J. Velasco-Vélez, R. V. Mom, A. Knop-Gericke, R. Schlögl, D. Teschner and T. E. Jones, *Curr. Opin. Electrochem.*, 2021, **30**, 100842
6. Q. Feng, X.-Z. Yuan, G. Liu, B. Wei, Z. Zhang, H. Li and H. Wang, *J. Power Sources*, 2017, **366**, 33
7. Y. Jiao, Y. Zheng, M. Jaroniec and S.-Z. Qiao, *Chem. Soc. Rev.*, 2015, **44**, (8), 2060
8. J. Shan, Y. Zheng, B. Shi, K. Davey and S.-Z. Qiao, *ACS Energy Lett.*, 2019, **4**, (11), 2719
9. K. Schweinar, B. Gault, I. Mouton and O. Kasian, *J. Phys. Chem. Lett.*, 2020, **11**, (13), 5008
10. A. Zagalskaya, I. Evazzade and V. Alexandrov, *ACS Energy Lett.*, 2021, **6**, (3), 1124
11. A. Zagalskaya and V. Alexandrov, *ACS Catal.*, 2020, **10**, (6), 3650
12. K. Sardar, E. Petrucco, C. I. Hiley, J. D. B. Sharman, P. P. Wells, A. E. Russell, R. J. Kashtiban, J. Sloan and R. I. Walton, *Angew. Chem. Int. Ed.*, 2014, **53**, (41), 10960
13. D. L. Burnett, E. Petrucco, A. E. Russell, R. J. Kashtiban, J. D. B. Sharman and R. I. Walton, *Phys. Chem. Chem. Phys.*, 2020, **22**, (34), 18770
14. R. Kötz, H. Neff and S. Stucki, *J. Electrochem. Soc.*, 1984, **131**, (1), 72
15. H. G. Sanchez Casalongue, M. L. Ng, S. Kaya, D. Friebel, H. Ogasawara and A. Nilsson, *Angew. Chem. Int. Ed.*, 2014, **53**, (28), 7169
16. O. Kasian, J.-P. Grote, S. Geiger, S. Cherevko and K. J. J. Mayrhofer, *Angew. Chem. Int. Ed.*, 2018, **57**, (9), 2488
17. A. Minguzzi, O. Lugaresi, E. Achilli, C. Locatelli, A. Vertova, P. Ghigna and S. Rondinini, *Chem. Sci.*, 2014, **5**, (9), 3591
18. D. F. Abbott, D. Lebedev, K. Waltar, M. Povia, M. Nachtegaal, E. Fabbri, C. Copéret and T. J. Schmidt, *Chem. Mater.*, 2016, **28**, (18), 6591
19. A. R. Hillman, M. A. Skopek and S. J. Gurman, *Phys. Chem. Chem. Phys.*, 2011, **13**, (12), 5252
20. V. A. Saveleva, L. Wang, D. Teschner, T. Jones, A. S. Gago, K. A. Friedrich, S. Zafeiratos, R. Schlögl and E. R. Savinova, *J. Phys. Chem. Lett.*, 2018, **9**, (11), 3154
21. V. Pfeifer, T. E. Jones, S. Wrabetz, C. Massué, J. J. Velasco Vélez, R. Arrigo, M. Scherzer, S. Piccinin, M. Hävecker, A. Knop-Gericke and R. Schlögl, *Chem. Sci.*, 2016, **7**, (11), 6791
22. S. Geiger, O. Kasian, M. Ledendecker, E. Pizzutilo, A. M. Mingers, W. T. Fu, O. Diaz-Morales, Z. Li, T. Oellers, L. Fruchter, A. Ludwig, K. J. J. Mayrhofer, M. T. M. Koper and S. Cherevko, *Nat. Catal.*, 2018, **1**, (7), 508
23. L. She, G. Zhao, T. Ma, J. Chen, W. Sun and H. Pan, *Adv. Funct. Mater.*, 2022, **32**, (5), 2108465
24. S. Czioska, A. Boubnov, D. Escalera-López, J. Geppert, A. Zagalskaya, P. Röse, E. Saraçi, V. Alexandrov, U. Krewer, S. Cherevko and J.-D. Grunwaldt, *ACS Catal.*, 2021, **11**, (15), 10043
25. R. Kötz, S. Stucki, D. Scherson and D. M. Kolb, *J. Electroanal. Chem. Interfacial Electrochem.*, 1984, **172**, (1–2), 211
26. C. Spöri, J. T. H. Kwan, A. Bonakdarpour, D. P. Wilkinson and P. Strasser, *Angew. Chem. Int. Ed.*, 2017, **56**, (22), 5994
27. K. Hongsirikarn, J. G. Goodwin, S. Greenway and S. Creager, *J. Power Sources*, 2010, **195**, (21), 7213
28. T. Binninger, R. Mohamed, K. Waltar, E. Fabbri, P. Levecque, R. Kötz and T. J. Schmidt, *Sci. Rep.*, 2015, **5**, 12167
29. A. S. Raman and A. Vojvodic, *J. Phys. Chem. C*, 2022, **126**, (2), 922
30. N. Hodnik, P. Jovanovič, A. Pavlišič, B. Jozinović, M. Zorko, M. Bele, V. S. Šelih, M. Šala, S. Hočevar and M. Gaberšček, *J. Phys. Chem. C*, 2015, **119**, (18), 10140
31. Y. Liu, X. Liang, H. Chen, R. Gao, L. Shi, L. Yang and X. Zou, *Chin. J. Catal.*, 2021, **42**, (7), 1054
32. Y. Zhang, X. Zhu, G. Zhang, P. Shi and A.-L. Wang, *J. Mater. Chem. A*, 2021, **9**, (10), 5890
33. X.-K. Gu, J. C. A. Camayang, S. Samira and E. Nikolla, *J. Catal.*, 2020, **388**, 130
34. L. An, C. Wei, M. Lu, H. Liu, Y. Chen, G. G. Scherer, A. C. Fisher, P. Xi, Z. J. Xu and C.-H. Yan, *Adv. Mater.*, 2021, **33**, (20), 2006328
35. X. Miao, L. Zhang, L. Wu, Z. Hu, L. Shi and S. Zhou, *Nat. Commun.*, 2019, **10**, 3809
36. L. Zhang, H. Jang, Z. Li, H. Liu, M. G. Kim, X. Liu and J. Cho, *Chem. Eng. J.*, 2021, **419**, 129604
37. L. Wang, V. A. Saveleva, S. Zafeiratos, E. R. Savinova, P. Lettenmeier, P. Gazdzicki, A. S. Gago and K. A. Friedrich, *Nano Energy*, 2017, **34**, 385
38. Y. Lin, Z. Tian, L. Zhang, J. Ma, Z. Jiang, B. J. Deibert, R. Ge and L. Chen, *Nat. Commun.*, 2019, **10**, 162
39. L. Yang, G. Yu, X. Ai, W. Yan, H. Duan, W. Chen, X. Li, T. Wang, C. Zhang, X. Huang, J.-S. Chen and X. Zou, *Nat. Commun.*, 2018, **9**, 5236
40. Q. Zhang, X. Liang, H. Chen, W. Yan, L. Shi, Y. Liu, J. Li and X. Zou, *Chem. Mater.*, 2020, **32**, (9), 3904
41. L. C. Seitz, C. F. Dickens, K. Nishio, Y. Hikita, J. Montoya, A. Doyle, C. Kirk, A. Vojvodic, H. Y. Hwang, J. K. Norskov and T. F. Jaramillo, *Science*, 2016, **353**, (6303), 1011

 © 2022 Johnson Matthey

42. O. Diaz-Morales, S. Raaijman, R. Kortlever, P. J. Kooyman, T. Wezendonk, J. Gascon, W. T. Fu and M. T. M. Koper, *Nat. Commun.*, 2016, **7**, 12363
43. A. Grimaud, A. Demortière, M. Saubanère, W. Dachraoui, M. Duchamp, M.-L. Doublet and J.-M. Tarascon, *Nat. Energy*, 2016, **2**, (1), 16189
44. K. Sardar, S. C. Ball, J. D. B. Sharman, D. Thompsett, J. M. Fisher, R. A. P. Smith, P. K. Biswas, M. R. Lees, R. J. Kashtiban, J. Sloan and R. I. Walton, *Chem. Mater.*, 2012, **24**, (21), 4192
45. C. Shang, C. Cao, D. Yu, Y. Yan, Y. Lin, H. Li, T. Zheng, X. Yan, W. Yu, S. Zhou and J. Zeng, *Adv. Mater.*, 2019, **31**, (6), 1805104
46. J. Kim, P.-C. Shih, Y. Qin, Z. Al-Bardan, C.-J. Sun and H. Yang, *Angew. Chem. Int. Ed.*, 2018, **57**, (42), 13877
47. W. Sun, Y. Song, X.-Q. Gong, L. Cao and J. Yang, *ACS Appl. Mater. Interfaces*, 2016, **8**, (1), 820
48. R. Zhang, P. E. Pearce, V. Pimenta, J. Cabana, H. Li, D. A. D. Corte, A. M. Abakumov, G. Rousse, D. Giaume, M. Deschamps and A. Grimaud, *Chem. Mater.*, 2020, **32**, (8), 3499
49. R. Frydendal, E. A. Paoli, B. P. Knudsen, B. Wickman, P. Malacrida, I. E. L. Stephens and I. Chorkendorff, *ChemElectroChem*, 2014, **1**, (12), 2075
50. S. M. Alia, M.-A. Ha, G. C. Anderson, C. Ngo, S. Pylypenko and R. E. Larsen, *J. Electrochem. Soc.*, 2019, **166**, (15), F1243
51. D. L. Burnett, E. Petrucco, K. M. Rigg, C. M. Zalitis, J. G. Lok, R. J. Kashtiban, M. R. Lees, J. D. B. Sharman and R. I. Walton, *Chem. Mater.*, 2020, **32**, (14), 6150
52. H. A. El-Sayed, A. Weiß, L. F. Olbrich, G. P. Putro and H. A. Gasteiger, *J. Electrochem. Soc.*, 2019, **166**, (8), F458
53. A. Hartig-Weiss, M. F. Tovini, H. A. Gasteiger and H. A. El-Sayed, *ACS Appl. Energy Mater.*, 2020, **3**, (11), 10323
54. C. Wei, R. R. Rao, J. Peng, B. Huang, I. E. L. Stephens, M. Risch, Z. J. Xu and Y. Shao-Horn, *Adv. Mater.*, 2019, **31**, (31), 1806296
55. P. Aßmann, A. S. Gago, P. Gazdzicki, K. A. Friedrich and M. Wark, *Curr. Opin. Electrochem.*, 2020, **21**, 225
56. C. Van Pham, D. Escalera-López, K. Mayrhofer, S. Cherevko and S. Thiele, *Adv. Energy Mater.*, 2021, **11**, (44), 2101998
57. S. Trasatti, *J. Electroanal. Chem. Interfacial Electrochem.*, 1980, **111**, (1), 125
58. M. A. Hubert, A. M. Patel, A. Gallo, Y. Liu, E. Valle, M. Ben-Naim, J. Sanchez, D. Sokaras, R. Sinclair, J. K. Nørskov, L. A. King, M. Bajdich and T. F. Jaramillo, *ACS Catal.*, 2020, **10**, (20), 12182
59. D. F. Abbott, R. K. Pittkowski, K. Macounová, R. Nebel, E. Marelli, E. Fabbri, I. E. Castelli, P. Krtil and T. J. Schmidt, *ACS Appl. Mater. Interfaces*, 2019, **11**, (41), 37748
60. Q. Feng, J. Zou, Y. Wang, Z. Zhao, M. C. Williams, H. Li and H. Wang, *ACS Appl. Mater. Interfaces*, 2020, **12**, (4), 4520
61. N. Zhang, C. Wang, J. Chen, C. Hu, J. Ma, X. Deng, B. Qiu, L. Cai, Y. Xiong and Y. Chai, *ACS Nano*, 2021, **15**, (5), 8537
62. D. A. Kuznetsov, M. A. Naeem, P. V. Kumar, P. M. Abdala, A. Fedorov and C. R. Müller, *J. Am. Chem. Soc.*, 2020, **142**, (17), 7883
63. P. Wang, Q. Cheng, C. Mao, W. Su, L. Yang, G. Wang, L. Zou, Y. Shi, C. Yan, Z. Zou and H. Yang, *J. Power Sources*, 2021, **502**, 229903
64. F. Claudel, L. Dubau, G. Berthomé, L. Sola-Hernandez, C. Beauger, L. Piccolo and F. Maillard, *ACS Catal.*, 2019, **9**, (5), 4688
65. A. Zagalskaya and V. Alexandrov, *J. Phys. Chem. Lett.*, 2020, **11**, (7), 2695
66. A. Lončar, D. Escalera-López, S. Cherevko and N. Hodnik, *Angew. Chem. Int. Ed.*, 2022, **61**, (14), e202114437
67. D. L. Burnett, E. Petrucco, R. J. Kashtiban, S. F. Parker, J. D. B. Sharman and R. I. Walton, *J. Mater. Chem. A*, 2021, **9**, (44), 25114
68. D. Lebedev, M. Povia, K. Waltar, P. M. Abdala, I. E. Castelli, E. Fabbri, M. V. Blanco, A. Fedorov, C. Copéret, N. Marzari and T. J. Schmidt, *Chem. Mater.*, 2017, **29**, (12), 5182
69. C. W. Song, H. Suh, J. Bak, H. Bin Bae and S.-Y. Chung, *Chem*, 2019, **5**, (12), 3243
70. J. Edgington, N. Schweitzer, S. Alayoglu and L. C. Seitz, *J. Am. Chem. Soc.*, 2021, **143**, (26), 9961
71. R. Zhang, N. Dubouis, M. Ben Osman, W. Yin, M. T. Sougrati, D. A. D. Corte, D. Giaume and A. Grimaud, *Angew. Chem. Int. Ed.*, 2019, **58**, (14), 4571
72. N. Li, L. Cai, C. Wang, Y. Lin, J. Huang, H. Sheng, H. Pan, W. Zhang, Q. Ji, H. Duan, W. Hu, W. Zhang, F. Hu, H. Tan, Z. Sun, B. Song, S. Jin and W. Yan, *J. Am. Chem. Soc.*, 2021, **143**, (43), 18001
73. C.-L. Ma, Z.-Q. Wang, W. Sun, L.-M. Cao, X.-Q. Gong and J. Yang, *ACS Appl. Mater. Interfaces*, 2021, **13**, (25), 29654
74. Y. Chen, Y. Sun, M. Wang, J. Wang, H. Li, S. Xi, C. Wei, P. Xi, G. E. Sterbinsky, J. W. Freeland, A. C. Fisher, J. W. Ager, Z. Feng and Z. J. Xu, *Sci. Adv.*, 2021, **7**, (50), eabk1788
75. M. Ben-Naim, Y. Liu, M. B. Stevens, K. Lee, M. R. Wette, A. Boubnov, A. A. Trofimov, A. V. Ievlev, A. Belianinov, R. C. Davis, B. M. Clemens, S. R. Bare, Y. Hikita, H. Y. Hwang, D. C. Higgins, R. Sinclair and T. F. Jaramillo, *Adv. Funct. Mater.*, 2021, **31**, (34), 2101542

 © 2022 Johnson Matthey

76. M. Ji, X. Yang, S. Chang, W. Chen, J. Wang, D. He, Y. Hu, Q. Deng, Y. Sun, B. Li, J. Xi, T. Yamada, J. Zhang, H. Xiao, C. Zhu, J. Li and Y. Li, *Nano Res.*, 2022, **15**, (3), 1959
77. C. W. Song, J. Lim, H. Bin Bae and S.-Y. Chung, *Energy Environ. Sci.*, 2020, **13**, (11), 4178
78. W. Sun, J.-Y. Liu, X.-Q. Gong, W.-Q. Zaman, L.-M. Cao and J. Yang, *Sci. Rep.*, 2016, **6**, 38429
79. M. Retuerto, L. Pascual, O. Piqué, P. Kayser, M. A. Salam, M. Mokhtar, J. A. Alonso, M. Peña, F. Calle-Vallejo and S. Rojas, *J. Mater. Chem. A*, 2021, **9**, (5), 2980
80. T. Reier, D. Teschner, T. Lunkenbein, A. Bergmann, S. Selve, R. Kraehnert, R. Schlögl and P. Strasser, *J. Electrochem. Soc.*, 2014, **161**, (9), F876
81. H.-S. Oh, H. N. Nong, T. Reier, A. Bergmann, M. Gliech, J. Ferreira de Araújo, E. Willinger, R. Schlögl, D. Teschner and P. Strasser, *J. Am. Chem. Soc.*, 2016, **138**, (38), 12552
82. C. D. F. da Silva, F. Claudel, V. Martin, R. Chattot, S. Abbou, K. Kumar, I. Jiménez-Morales, S. Cavaliere, D. Jones, J. Rozière, L. Solà-Hernandez, C. Beauger, M. Faustini, J. Peron, B. Gilles, T. Encinas, L. Piccolo, F. H. Barros de Lima, L. Dubau and F. Maillard, *ACS Catal.*, 2021, **11**, (7), 4107
83. J. Kibsgaard and I. Chorkendorff, *Nat. Energy*, 2019, **4**, (6), 430
84. M. You, L. Gui, X. Ma, Z. Wang, Y. Xu, J. Zhang, J. Sun, B. He and L. Zhao, *Appl. Catal. B: Environ.*, 2021, **298**, 120562
85. J. Joo, Y. Park, J. Kim, T. Kwon, M. Jun, D. Ahn, H. Baik, J. H. Jang, J. Y. Kim and K. Lee, *Small Methods*, 2021, **6**, (1), 2101236
86. M. Kim, J. Park, M. Kang, J. Y. Kim and S. W. Lee, *ACS Cent. Sci.*, 2020, **6**, (6), 880

The Authors

Jasmine Clayton studied Chemistry at the University of Warwick, UK, graduating with MChem (Hons) in 2019. As a Masters student she undertook an international placement at the University of Modena and Reggio Emilia, Italy, under the supervision of Alfonso Zambon. Her final year research project on gallium substituted AlPO zeotypes was under the supervision of Professor Richard Walton. She is presently undertaking research for a PhD in collaboration with Johnson Matthey on acid-resilient OER catalysts and catalyst supports.

Richard Walton is Professor of Chemistry at the University of Warwick, and director of Warwick's X-ray facility. His research group investigate the synthesis and structures of inorganic materials, particularly from solution-based crystallisation, such as hydrothermal chemistry. This includes open-framework zeotypes and MOFs, as well as condensed oxide structures, that may have practical applications in areas related to energy and heterogeneous catalysis. He has collaborated with various scientists at Johnson Matthey for the past 20 years, and was Royal Society Industry Fellow from 2015–2019 at Johnson Matthey.

© 2022 Johnson Matthey